Generation of 656 nm coherent red-light by frequency-doubled Nd:YLiF4/β-BaB2O4 laser for a compact silver atoms optical clock

J.-P. Loisel, Suat Topsu, Luc Chassagne, Yasser Alayli, Pierre-Richard Dahoo, Patrick Juncar

Int. J. Metrol. Qual. Eng. **3**, 7–13 (2012)

DOI: 10.1051/ijmqe/2012008

Generation of 656 nm coherent red-light by frequency-doubled Nd:$YLiF_4$/β-BaB_2O_4 laser for a compact silver atoms optical clock

J.-P. Loisel[1], S. Topsu[1,*], L. Chassagne[1], Y. Alayli[1], P.R. Dahoo[2], and P. Juncar[3]

[1] LISV, University of Versailles, 78035 Versailles, France
[2] CNRS/Insu LATMOS-IPSL, University of Versailles, 78280 Guyancourt, France
[3] LNE-INM/CNAM, 93210 Saint-Denis, France

Received: 26 March 2012 / Accepted: 26 March 2012

Abstract. We describe an efficient continuous-wave diode-pumped Nd:$YLiF_4$ laser oscillating on the σ-polarized $^4F_{3/2}$–$^4I_{13/2}$ transition at $\lambda_\omega = 1312$ nm. With a simple linear cavity laser, we reached an intracavity power of 310 W at $\lambda = 1312$ nm for 16 W of absorbed pump power ($\lambda_p \sim 806$ nm). A 0.25 W of tunable radiation ($\lambda_{2\omega} = 656$–658 nm) was obtained by intracavity second-harmonic generation (SHG) with a $5 \times 5 \times 7$ mm^3 β-BaB_2O_4 crystal. Up to 10 mW of tunable single-frequency operation was observed using a 200 μm thin fused silica intracavity solid etalon. The optimal waist for a maximum conversion efficiency has been calculated theoretically using Boyd and Kleiman model. For the 1312–656 nm SHG, we found a walk-off parameter $B = 8.99$ and an optimal waist of 25 μm. Comparing to the experimental measurement of the optimal waist, we found a relative discrepancy of 2.84×10^{-2}. This laser is dedicated to the spectroscopic study of silver atoms trapped in a buffer-gas-free paraffin coated Pyrex cell that will be used in a compact atomic optical clock.

Keywords: Laser; optical clock; spectroscopic; diode-pumped solid-stage

1 Introduction

Microwave atomic clocks have been the standards for precision time and frequency metrology over the past 50 years [1], finding widespread use in basic scientific studies, communications, and navigation. Compact and robust apparatus are widely commercially available today. With its higher operating frequency, an atomic clock based on an optical transition can be much more stable. Optical standards based on a single ion [2–6] or a collection of laser-cooled atoms could reach a stability as low as $\sigma \sim 10^{-18}$ (rather than $\sigma \sim 10^{-11}$ for a microwave atomic clock). Several atoms are under study to replace Cesium [7]. Silver atoms based atomic clocks are between the most promising candidates [8–10]. The natural spectral linewidth of the clock transition $4d^{10}5s\ ^2S_{1/2} \rightarrow 4d^9 5s^2\ ^2D_{5/2}$ has been estimated to 0.8 Hz, calculated theoretically using multiconfigurational Fermi-Dirac method [11]. This long-lived state is accessible from the ground state $5s\ ^2S_{1/2}$ with a two-photon transition at 661.2 nm, providing a first-order Doppler-free interaction with atoms of all velocities [10, 12]. Furthermore, the nuclear spin $I = 1/2$ of the two stable isotopes ^{107,109}Ag induces a hyperfine structure which allows transitions between levels with $m_F = 0$ and thus are insensitive to the first order Zeeman effect. The improvement in term of accuracy and stability is made at the cost of the compactness. Actually, atom species that present interesting optical transition clock are obtained from an oven put under a high-vacuum chamber. This constraint makes difficult the development of compact optical atomic clocks that could one day replace microwave atomic clocks in geopositionning or other systems where compactness and portability are required.

On the other way, since 1993 a non-thermal desorption process of atoms in Pyrex cells from the use of low intensity light source has been studied and developed [13, 14]. This process, named LIAD for light induced atomic desorption, has been observed for Na, K, Rb and Cs atoms desorbed by weak illumination of cells coated with polydimethylsiloxane, octamethylcyclotetrasiloxane and paraffin [15–19]. It is commonly used for efficient loading of magneto-optical via quantum jump spectroscopy [20,21]. State of art and on LIAD and related phenomena is reported in [22].

We though that the preparation of high density with a low kinetic energy atomic samples using LIAD effect and buffer-gas-free paraffin coated cells represents an attractive way for compact optical atomic clocks. For this purpose, we built a buffer-gas-free paraffin coated Pyrex cell filled with silver atoms [23]. We demonstrated

* Correspondence: suat.topsu@uvsq.fr

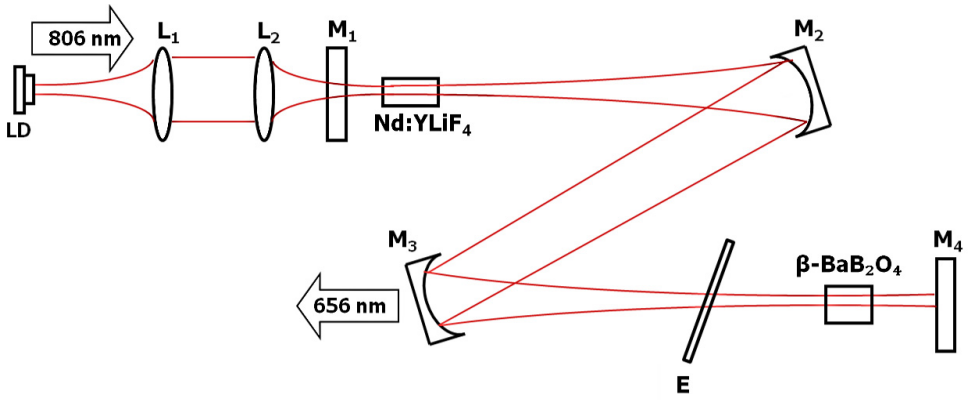

Fig. 1. (Color online) Setup of the cw-diode pumped Nd:$YLiF_4$/β-BaB_2O_4 for the generation of single frequency radiation at $\lambda_{2\omega} = 656$ nm. LD: Laser Diode, L_1: Lens, L_2: Lens, M_1: Mirror (HT 806 nm, HR 1312 nm), M_2: Mirror (HR 1312 nm), M_3: Mirror (HT 656 nm, HR 1312 nm), M_4: Mirror (HT 656 nm, HR 1312 nm).

qualitatively the presence of LIAD effect on silver atoms by measuring the variation of the coefficient transmission of the thin film of silver atoms and paraffin, illuminated by a power-controlled argon laser source. To study quantitatively this process, i.e. the measurement of the desorption rate and the relative vapor density variation as a function of the desorbing light intensity and frequency, we need a laser source with a frequency corresponding to a dipolar transition in silver atoms. The most interesting transition is the $4d^{10}5s^2S_{1/2}$–$4d^{10}5p\ ^2P_{3/2}$ dipolar transition with a corresponding wavelength of $\lambda = 328.162$ nm and a natural spectral linewidth of 23 MHz. Frequency stabilized laser diodes at $\lambda = 656.324$ nm would be the most convenient to use but to our knowledge, they lack the necessary power for the generation of some milliwatts at 328 nm. Furthermore, with Nd doped crystals it is possible to achieve high finesse cavities with high intracavity power, because of moderate gain and large saturation intensity.

We chose to obtain some milliwatts of red radiation by second harmonic generation (SHG) of a laser source at 1312 nm by intracavity doubling and simple linear cavity [24–26]. High power TEM_{00} 656 nm red line laser source has been demonstrated from a Nd:$YLiF_4$ crystal as a gain element and an unidirectional ring laser [27,28]. They are based on complex configurations that leads to unstable and unreliable devices and they are subject to thermal effects of the laser crystal. Furthermore, in our experiment, robustness and stable operating systems are more important than high power. Hence, we chose to develop a simple linear cavity although it is well known that a diode-pumped solid-state laser employing a linear standing-wave resonator cannot operate in a single-longitudinal mode operation due to spatial mode-burning effects stemming from the standing-waves. In this paper, we demonstrate that the hole burning effect is not always a limitation for a linear cavity laser where SHG frequency conversion is used. With a simple linear cavity Nd:$YLiF_4$/β-BaB_2O_4 continuous-wave (cw) laser investigated at 1312 nm, we have obtained an output power of 3.6 W at 1312 nm for 13.8 W of absorbed pump power ($\lambda_p \sim 806$ nm). A 0.25 W of tunable radiation ($\lambda_{2\omega} = 656$–658 nm) was obtained by intracavity SHG with a $5 \times 5 \times 7$ mm^3 β-BaB_2O_4 crystal. Up to 10 mW of tunable single-frequency operation was observed using an intracavity solid etalon.

2 The cw-Nd:$YLiF_4$/β-BaB_2O_4 laser setup

The Nd:$YLiF_4$ laser crystal offers two advantages, compared to the well-known Nd-YAG crystal - low thermal lensing and negligible thermal birefringence [29,30] which represent an important point for high-power TEM_{00} operation. To generate some milliwatt levels of UV power from external ring cavity SHG in a β-BaB_2O_4 nonlinear crystal, a minimum red power of 10 to 20 mW should be available. In this section, we report the theoretical approach for the realization of a 1312 μm$\rightarrow$656 nm optimal doubling cavities. Because the transition levels $^4F_{3/2}$ –$^4I_{13/2}$ at $\lambda = 1312.648$ nm does not match the gain line center, the stimulated cross-section is reduced by 30% to $\sigma_{em} = 1.5 \times 10^{-20}$ cm^2, a 10 times weaker than that of the main σ-emission line at 1053 nm. We choose to make the generation of a single-frequency red source at 656.3 nm by an intracavity SHG approach. The key points of the developed laser source are the use of a cw diode-pumped crystal Nd:$YLiF_4$ linear laser cavity with β-BaB_2O_4 crystal as the frequency-doubling element ($\lambda = 656$ nm). The setup of the simple linear resonator is illustrated in Figure 1.

In order to maximize the conversion efficiency we calculated the optimal waist in the β-BaB_2O_4 crystal. For this purpose, we used the ABCD matrix and Boyd and Kleinman theories as reported in [31]. Let us consider a Gaussian pump beam focused at the center of a nonabsorbing crystal. According to the usual notation, k_1 is the longitudinal wavenumber of the light at the fundamental frequency $\omega = k_1 c/n_1$ propagating in a crystal of refractive index n_1. The beam radius w_0 at its waist, is assumed to be located in the central plane $z = l/2$ of the crystal

of length l. The factor $\tau = (2z - l)/b$, where $b = w_0^2 k_1$ is the confocal parameter. It describes the evolution of the beam size and wavefront curvature in the course of propagation, following the usual Gaussian-beam theory. In these conditions, the Boyd and Kleinman calculations predict the conversion efficiency η for the second harmonic generation of light at the frequency 2ω with wavenumber $k_2 = 2\omega n_2/c$. It is equal to

$$\eta = \frac{P_{2\omega}}{P_\omega} = \frac{2\omega^3 l d_{eff}^2}{\pi\varepsilon_0 c^4 n_1 n_2} h(\sigma, B, \xi) P_\omega \qquad (1)$$

where d_{eff}(pm/V) is the effective second-order polarization coefficient of the crystal, P_ω and $P_{2\omega}$ are respectively, the powers of the pump and of the SHG beams. The function $h(\sigma, B, \xi)$ is defined as

$$h(\sigma, B, \xi) = \frac{1}{4\xi} \int_{-\xi}^{+\xi} \int_{-\xi}^{+\xi} \frac{e^{i\sigma(\tau-\tau')} e^{-B^2(\tau-\tau')^2/\xi}}{(1+i\tau)(1-i\tau')} d\tau d\tau'. \qquad (2)$$

This function weights the contributions of the harmonic power arising at different longitudinal locations inside the crystal. The quantities upon which h depends are the focusing parameter $\xi = l/b$, the normalized mismatch $\sigma = b\Delta k/2$ where $\Delta k = |2k_1 - k_2|$, and the nondimensional walk-off parameter B defined as $B = (\rho/2)\sqrt{lk_1}$ for a crystal having a walk-off angle ρ. It is practically always of interest to optimize the SHG efficiency with respect to the mismatch parameter σ. For this purpose the function $h_m(B, \xi) = \max\{h(\sigma, B, \xi)\}_\sigma$ is used instead of equation (2). The walk-off parameter and the focusing parameter depend on the crystal length. When B satisfies the wide range of focusing conditions expressed by $4B^2 > \xi > 6/B^2$, in this case h_m is given by [31]

$$h_m(B, \xi) = (\omega_y/\omega_x)^{1/2} (l_a/l) \tan^{-1} \xi \qquad (3)$$

where ω_x and ω_y are the beam waists of the focused beams in the horizontal and vertical planes and $l_a = \sqrt{\pi}\omega_x/\rho$ is the aperture length.

We applied this calculus in two cases: first one with a 7 mm long β-BaB_2O_4 crystal for a 1312−656 nm SHG and for a 10 mm length β-BaB_2O_4 crystal for a 656−328 nm SHG that will be useful to excite the dipolar transition $^2S_{1/2}$−$^2P_{3/2}$ in silver atoms. The theoretical results for both cases are reported in Figure 2.

We found the maximum of the h_m functions for a focusing parameter $\xi_M = 1.392$. Then the optimal waist is deduced from

$$\omega_0 = \sqrt{l\lambda_\omega / 2\pi n_o(\lambda_\omega)\xi}. \qquad (4)$$

For the 1312−656 nm SHG, we have a walk-off parameter $B = 8.99$ and an optimal waist of 25 μm. For the 656−328 nm SHG, we obtained a walk-off parameter $B = 14.89$ and an optimal waist of 21.2 μm. We emphasize that for both values of B, the condition $4B^2 > \xi > 6/B^2$ is satisfied which is required to validate the use of equation (3).

In order to estimate the uncertainty on these values due to the approximation (Eq. (3)), we made a series of slope efficiency measurements to determine experimentally the optimal waist for the 656−328 nm SHG.

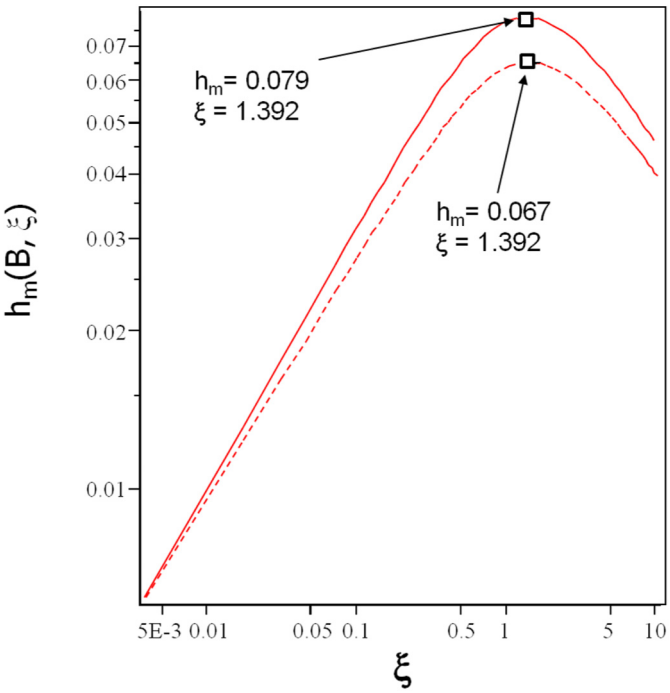

Fig. 2. (Color online) Results of the calculus of the $h_m(B, \xi)$ functions for 1312−656 nm SHG with $B = 8.99$ (straight line) and for 656−328 nm SHG with $B = 14.89$ (dashed line).

For this purpose, we used an extended cavity laser diode (ECLD) (LD100, Toptica) emitting around 656.3 nm. The monomode behavior of the laser source is controlled thanks to a Fabry Pérot cavity. A wavemeter (WA1000, Burleigh) is used to control and to adjust its wavelength to 656.324 nm using the current control of the laser and the voltage control of the piezoelectric actuator. As the beam issue from the ECLD source is strongly elliptical, an anamorphic prism is used for approaching a Gaussian mode. The β-BaB_2O_4 crystal used in our experiment is a θ-cut one with $\varphi = 30°$. The phase-matching angle is 36.3° and its size is $4 \times 4 \times 10$ mm^3. Both faces of the crystal are coated antireflection around 656 nm and 328 nm. Although we used an ultraviolet sensitive photodiode, an optical low-pass filter ($\lambda_{cut} \sim 656$ nm) is placed just before the photodiode. The measurements have been made for several waist sizes up to 44 μm. The experimental setup is given in Figure 3 and results for two cases $\omega_0 = 21.8$ μm and $\omega_0 = 43.9$ μm are reported in Figure 4. These waists correspond to the maximum and the minimum values of η according our measurement range.

We observed SHG conversion efficiencies that vary from $4.5(1) \times 10^{-2}$ at least ($\omega_0 = 43.9$ μm, circle symbols) to $9.8(1) \times 10^{-2}$ at best ($\omega_0 = 21.8$ μm, triangle symbols). From the experimental value of 21.8 μm and in regard to the theoretical value of 21.2 μm calculated before, we can deduce that the relative uncertainty on the model of Boyd and Kleinman due to approximation of equation (3) is about 2.84×10^{-2}.

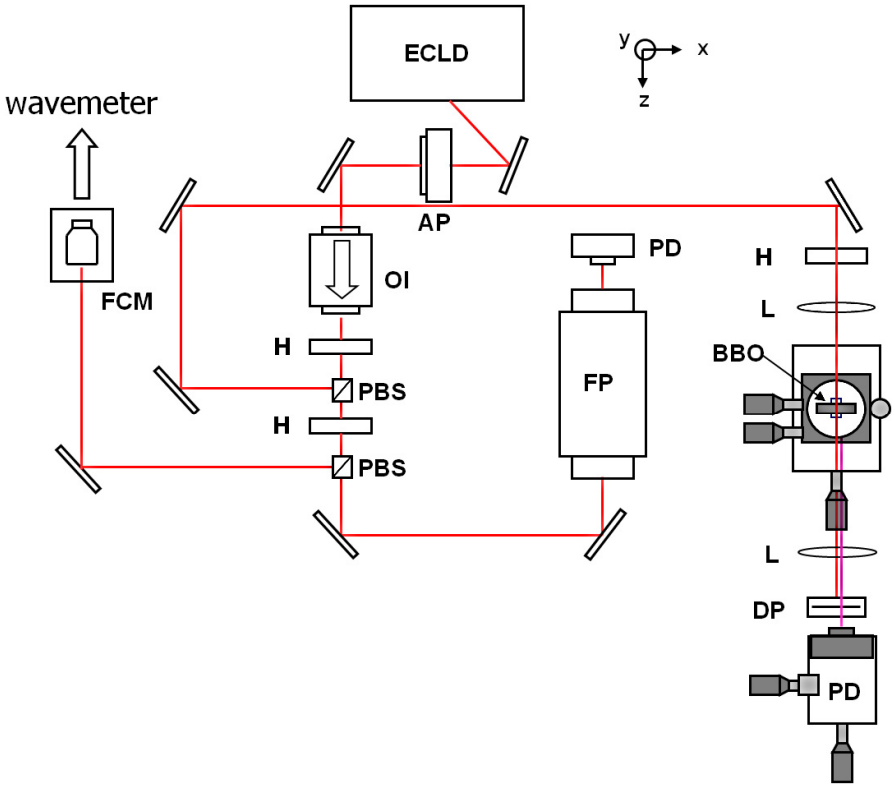

Fig. 3. (Color online) Experimental setup used for the measurement of the SHG conversion efficency according to the waist size. AP: Anamorphic prism, BBO: β-BaB_2O_4 crystal, ECLD: Extended cavity laser diode, DP: Dichroic waveplate, FCM: three axis fiber coupling mount, FP: Fabry Pérot cavity, H: Half-waveplate, L: Lens, M: mirrors, OI: Optical isolator, PBS: Polarization beamsplitter, PD: Photodiode.

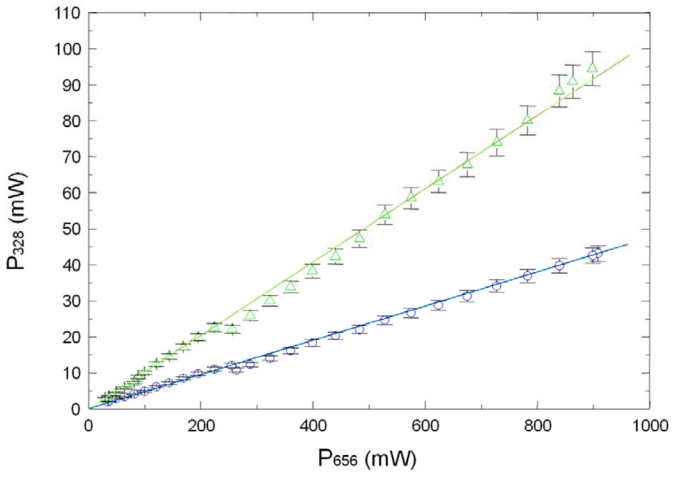

Fig. 4. (Color online) SHG conversion efficiencies in a β-BaB_2O_4 crystal for a waist value of $\omega_0 = 43.9$ μm ($\circ$) and of $\omega_0 = 21.8$ μm ($\triangle$).

3 Realization and characterization of the Nd:$YLiF_4$/β-BaB_2O_4 laser

The laser gain medium is a α-cut, 0.82% Nd^{3+}-doped $YLiF_4$ crystal (Fig. 5). Its size is $3\times3\times10$ mm^3. The crystal is coated antireflection around 806 nm and 1312 nm. The pump source is a 25 W fiber-coupled diode (Limo F200-DL808) with a central wavelength equal to 806 nm for a temperature of 17.5 °C. The numerical aperture of the output fiber is 0.22 and its core diameter is 200 μm. The pump focusing optics consist of two doublets. The first doublet with a 60 mm focal length is used to collimate the pump beam. The crystal is wrapped in an indium foil and it is mounted in a copper heat sink whose temperature is controlled with a water circulation at 8 °C. Our system is similar to those described in [27]. The second doublet (f_2 = 100 mm) is used to focus the pump beam in the Nd:$YLiF_4$ crystal with a waist of $w_o = 180$ μm. The crystal's absorption rate is 80%. The mirrors M1 ($R = -500$ mm), M2 ($R = -300$ mm) and M3 ($R = -200$ mm) are coated to obtain high reflection around 1312 nm. The outcoupling plan-mirror M4 has a transmission of $T = 0.1\%$ permitting an accurate evaluation of the intracavity power. The doubling crystal is a β-BaB_2O_4 crystal, θ-cut with a phase-matching angle of 20.3°, $\varphi = 0°$, $5\times5\times7$ mm^3, antireflection coated around 1312 nm and 656 nm.

Figure 6 shows the multimode infrared ($\lambda_\omega = 1312$ nm, square symbols) and red ($\lambda_{2\omega} = 656$ nm, triangle symbols) output characteristics of the laser. We reached an intracavity power of 310 W for 16 W of absorbed pump power ($\lambda_p \sim 806$ nm). Up to 0.25 W tunable multi-frequency laser ($\lambda_{2\omega} = 656{-}658$ nm) is observed. Figure 7 displays

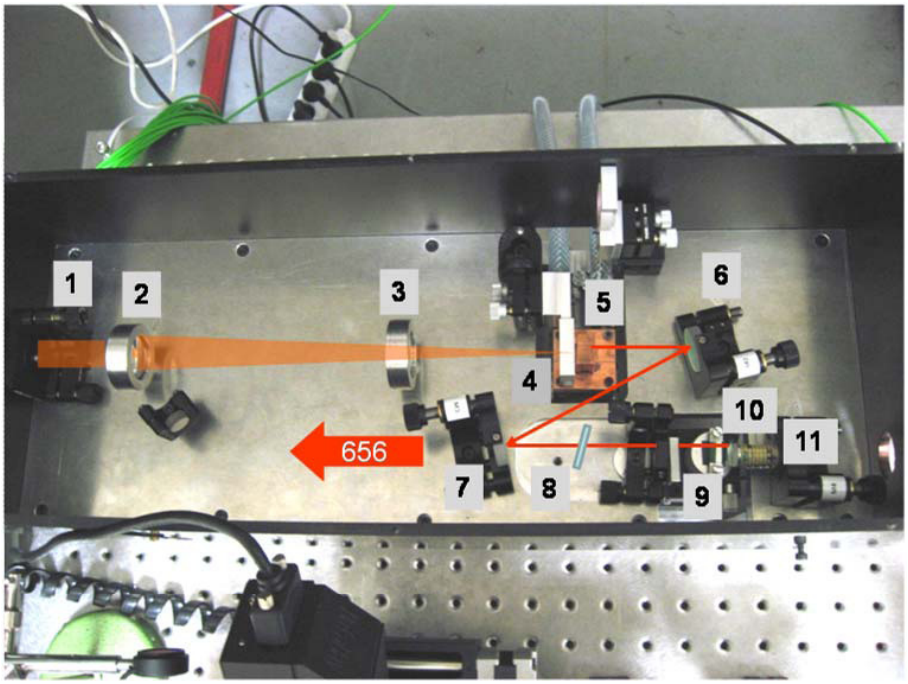

Fig. 5. (Color online) Photography of the Nd:$YLiF_4$/β-BaB_2O_4 linear cavity laser. 1: Diode pump, 2: Lens, 3: Lens, 4: Mirror M_1, 5: Nd:$YLiF_4$ crystal, 6: Mirror M_2, 7: Mirror M_3, 8: Fused silica etalon, 9: β-BaB_2O_4 crystal, 10: Mirror M_4, 11: Piezoelectric actuator.

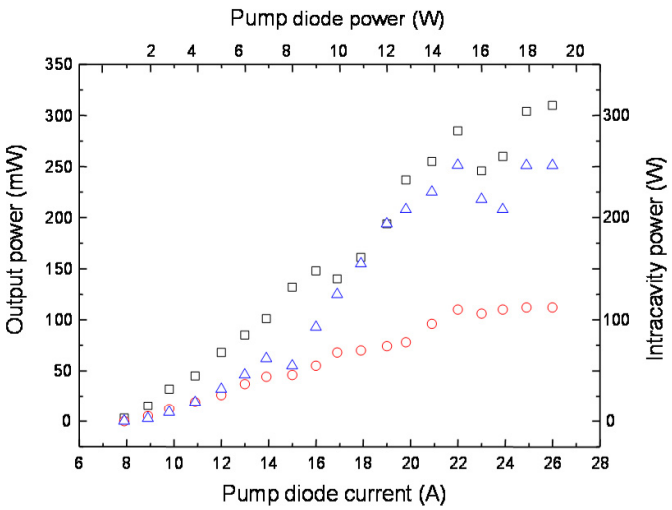

Fig. 6. (Color online) Power characteristics at $\lambda_\omega = 1312$ nm without an intracavity etalon (□), at $\lambda_\omega = 1312$ nm with an intracavity etalon (○) and at $\lambda_{2\omega} = 656$ nm without an intracavity etalon (△) versus diode current. Output power (left axis) and intracavity power (right axis).

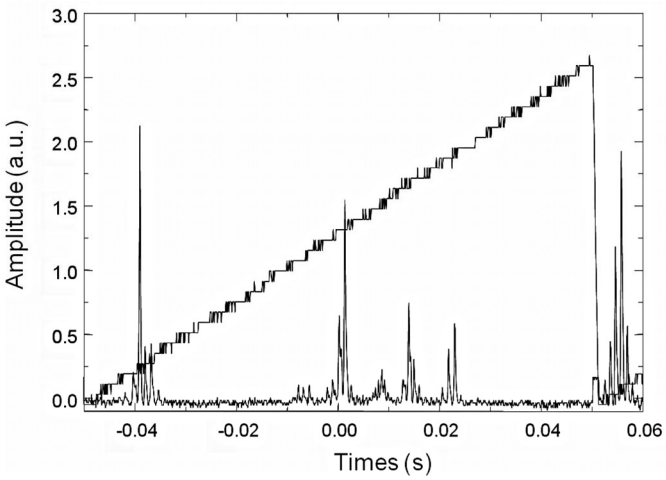

Fig. 7. Output of the scanning confocal Fabry Pérot analyzer showing the multilongitudinal modes of the linear cavity laser at $\lambda_{2\omega} = 656$ nm.

the associated longitudinal mode spectra as analyzed by a scanning confocal Fabry Pérot interferometer with a free spectral range of 1500 MHz. Without an etalon, the laser spontaneously oscillated over several longitudinal modes at the gain center. The intracavity power tends to saturate at large absorbed pump power due to the combined effects of thermal lensing caused both by the Nd:$YLiF_4$ and β-BaB_2O_4 crystals and thermal depolarization in the Nd:$YLiF_4$.

To obtain a single frequency laser, we use a thin fused silica etalon with a free-spectral range of 1.5 nm. This permits a quasi-continuous tuning of the wavelength within the gain profile. Figure 8 displays the single longitudinal mode spectra given by the scanning confocal Fabry Pérot. The etalon loss combined with the reduced

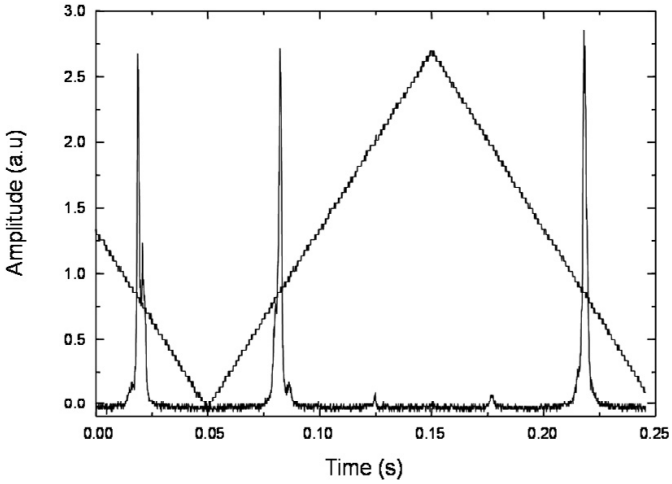

Fig. 8. Output of the scanning confocal Fabry Pérot analyser showing a single-frequency operation of the linear cavity laser at $\lambda_{2\omega} = 656$ nm.

emission cross-section at 1312 nm results in a decrease of the intracavity power to 110 W for 16 W of absorbed pump power (Fig. 5, circle symbols). Furthermore, with a small gain region located at one end of the cavity, spatial hole burning problems are reduced [32]. The maximum output power obtained in a single-frequency mode is about 10 mW for a fused silica etalon with a 200 μm thickness and $R = 25\%$. This demonstrates that the hole burning effect is not always a limitation for a linear cavity laser where SHG frequency conversion is used.

4 Conclusion

This paper provides the demonstration that when high power is not the chief criteria, a simple linear cavity with an intracavity SHG of diode-pumped Nd:$YLiF_4$ lasers at 1312 nm is not limited by the hole burning effect or thermal lenses. In a standing-wave cavity configuration, we have achieved 310 W of multimode TEM_{00} intracavity at 1312 nm for 16 W of absorbed pump power. A 10 mW single-frequency operation tunable between 656−658 nm has been obtained by intracavity SHG. We also report the experimental measurement of the red-uv conversion efficiency of the β-BaB_2O_4 crystal according to the waist size in the crystal. Obtained values are in good agreement on about 2% with those calculated by the Boyd and Kleinman theory. Finally, we note that diode-pumped solid-state lasers near 1312 nm are appropriate for the spectroscopic study of Ag atoms at 328 nm but also for Na atoms at the 657 nm intercombination line.

Acknowledgements. The authors are grateful to F. Mourgues for its contribution to this works.

References

1. L. Essen, D.S. Sutcliffen, Improvement to the national physical laboratory atomic clock, Nature **223**, 602−603 (1969)
2. H.S. Margolis, G.P. Barwood, G. Huang, H.A. Klein, S.N. Lea, K. Szymaniec, P. Gill, Hertz-level measurement of the optical clock frequency in a single $^{88}Sr^+$ ion, Science **306**, 1355 (2004)
3. G.P. Barwood, H.S. Margolis, G. Huang, P. Gill, H.A. Klein, Measurement of the electric quadrupole moment of the $4d^2D_{5/2}$ level in $^{88}Sr^+$, Phys. Rev. Lett. **93**, 133001 (2004)
4. T. Schneider, E. Peik, C. Tamm, Sub-Hertz optical frequency comparisons between two trapped $^{171}Yb^+$ ions, Phys. Rev. Lett. **94**, 230801 (2005)
5. W.H. Oskay, W.M. Itano, J.C. Bergquist, Measurement of the $^{199}Hg^+$ $5d^9$ $6s^2$ $^2D_{5/2}$ electric quadrupole moment and a constraint on the quadrupole shift, Phys. Rev. Lett. **94**, 163001 (2005)
6. P. Dube, A.A. Madej, J.E. Bernard, L. Marmet, J.-S. Boulanger, S. Cundy, Electric quadrupole shift cancellation in single-ion optical frequency standards, Phys. Rev. Lett. **95**, 033001 (2005)
7. W.H. Oskay, S.A. Diddams, E.A. Donley, T.M. Fortier, Single-atom optical clock with high accuracy, Phys. Rev. Lett. **97**, 020801 (2006)
8. T. Badr, M.D. Plimmer, P. Juncar, M.E. Himbert, Y. Louyer, D.J.E. Knight, Observation by two-photon laser spectroscopy of the $4d^{10}5s$ $^2S_{1/2}$ $\rightarrow 4d^9 5s^2$ $^2D_{5/2}$ clock transition in atomic silver, Phys. Rev. A **74**, 062509 (2006)
9. G. Uhlenberg, J. Dirscherl, H. Walther, Magneto-optical trapping of silver atoms, Phys. Rev. A **62**, 063404 (2000)
10. P.L. Bender, J.L. Hall, R.H. Garstang, F.M.J. Pichanik, W.W. Smith, R.L. Barger, J.B. West, Candidates for two-photon optical frequency standards, Bull. Am. Phys. Soc. **21**, 599 (1976)
11. S. Topcu, J. Nasser, L.M.L. Daku, S. Fritzsche, Ab initio calculations of external-field shifts of the 661-nm quadrupolar clock transition in neutral Ag atoms, Phys. Rev. A **73**, 42503 (2006)
12. W.M. Itano, J.C. Bergquist, R.G. Hulet, D.J. Wineland, Radiative decay rates in Hg^+ from observations of quantum jumps in a single ion, Phys. Rev. Lett. **59**, 2732 (1987)
13. S. Gozzini, G. Nienhuis, E. Mariotti, G. Paffuti, C. Gabbanini, L. Moi, Wall effects on light induced drift, Opt. Commun. **88**, 341 (1992)
14. M. Meucci, E. Mariotti, P. Bicchi, C. Marinelli, L. Moi, Light-induced atom desorption, Europhys. Lett. **25**, 639 (1994)
15. E. Mariotti, S. Atutov, M. Meucci, P. Bicchi, C. Marinelli, L. Moi, Dynamics of rubidium light-induced atom desorption (LIAD), Chem. Phys. **187**, 111 (1994)
16. S.N. Atutov, V. Biancalana, P. Bicchi, C. Marinelli, E. Mariotti, M. Meucci, A. Nagel, K. Nasyrov, S. Rachini, L. Moi, Light induced diffusion and desorption of alkali metals in a siloxane film: theory and experiment, Phys. Rev. A **60**, 4693 (1999)
17. C. Marinelli, K.A. Nasyrov, S. Bocci, B. Pieragnoli, A. Burchianti, V. Biancalana, E. Mariotti, S.N. Atutov, L. Moi, A new class of photo-induced phenomena in siloxane films, Eur. Phys. J. D **13**, 231 (2001)

18. S. Gozzini, A. Lucchesini, Light-induced potassium desorption from polydimethylsiloxane film, Eur. Phys. J. D **28**, 157 (2004)
19. E.B. Alexandrov, M.V. Balabas, D. Budker, D. English, D.F. Kimball, C.-H. Li, V.V. Yashchuk, Light-induced desorption of alkali-metal atoms from paraffin coating, Phys. Rev. A **66**, 042903 (2002)
20. B.P. Anderson, M.A. Kasevich, Loading a vapor-cell magneto-optic trap using light-induced atom desorption, Phys. Rev. A **63**, 023404 (2001)
21. S.N. Atutov, R. Calabrese, B. Guidiai, A.G. Rudavets, E. Scansani, L. Tomassetti, V. Biancalana, A. Burchianti, C. Marinelli, E. Mariotti, L. Moi, S. Veronesi, Fast and efficient loading of a Rb magneto-optical trap using light-induced atomic desorption, Phys. Rev. A **67**, 053401 (2003)
22. A. Burchianti, A. Bogi, C. Marinelli, E. Mariotti, L. Moi, Light-induced atomic desorption and related phenomena, Phys. Scr. T **135**, 014012 (2009)
23. J.-P. Loisel, *Réalisation de sources laser à l'état solide et observation du phénomène LIAD : application au développement d'une horloge optique à atomes neutres d'argent*, Doctoral thesis, University of Versailles, 2010
24. Y. Louyer, F. Balembois, M.D. Plimmer, T. Badr, P. Georges, P. Juncar, M.E. Himbert, Efficient cw operation of diode-pumped Nd:YLF lasers at 1312.0 and 1322.6 nm for a silver atom optical clock, Opt. Commun. **217**, 357−362 (2003)
25. Y. Louyer, P. Juncar, M.D. Plimmer, T. Badr, F. Balembois, P. Georges, M.E. Himbert, Doubled single-frequency Nd:YLF ring laser coupled to a passive nonresonant cavity, Appl. Opt. **43**, 1773 (2004)
26. F. Balembois, D. Boutard, E. Barnasson, M. Baudrier, R. Paries, C. Schwach, S. Forget, Efficient diode-pumped intracavity frequency-doubled cw Nd:YLF laser emitting in the red, Opt. Laser Technol. **38**, 626–630 (2006)
27. R. Sarrouf, V. Sousa, T. Badr, G. Xu, J.-J. Zondy, Watt-level single-frequency tunable Nd:YLF/periodically poled $KTiOPO_4$ red laser, Opt. Lett. **32**, 2732 (2007)
28. R. Sarrouf, T. Badr, J.J. Zondy, Intracavity second-harmonic generation of diode-pumped continuous-wave single-frequency 1.3 μm Nd:$YLiF_4$ lasers, J. Opt. A: Pure Appl. Opt. **10**, 104011 (2008)
29. H. Vanherzeele, Thermal lensing measurement and compensation in a continuous-wave mode-locked Nd:YLF laser, Opt. Lett. **13**, 369 (1988)
30. V. Magni, G. Cerullo, S. De Silvestri, O. Svelto, L.J. Qian, M. Danailov, Intracavity frequency doubling of a cw high-power TEM_{00} Nd:YLF laser, Opt. Lett. **18**, 2111−2113 (1993)
31. G.D. Boyd, D.A. Kleinman, Parametric interaction of focused Gaussian light beams, J. Appl. Phys. **39**, 3597 (1968)
32. *Lasers*, edited by A.E. Siegman (University Science Books, 1986), Chap. 12